Radiology: Imaging Cancer

REVIEW

Quantitative MRI in Childhood Neuroblastoma: Beyond the Assessment of Image-defined Risk Factors

Haoru Wang, MD • *Jinhua Cai, MD, PhD*

From the Department of Radiology, Children's Hospital of Chongqing Medical University, National Clinical Research Center for Child Health and Disorders, Ministry of Education Key Laboratory of Child Development and Disorders, Chongqing Key Laboratory of Child Neurodevelopment and Cognitive Disorders, No. 136 Zhongshan Road 2, Yuzhong District, Chongqing 400014, China. Received March 28, 2024; revision requested May 15; revision received September 17; accepted October 2. **Address correspondence to** J.C. (email: *cai_jinhua@126.com*).

This study was funded by the Key Project of Technology Innovation and Application Development of Chongqing Science and Technology Bureau (no. CSTB2022TIADKPX0151).

Conflicts of interest are listed at the end of this article.

Radiology: Imaging Cancer 2024; 6(6):e240089 • https://doi.org/10.1148/rycan.240089 • Content codes: MR NR OI PD

Neuroblastoma commonly occurs in children. MRI is a radiation-free imaging modality and has played an important role in identifying image-defined risk factors of neuroblastoma, providing necessary guidance for surgical resection and treatment response evaluation. However, image-defined risk factors are limited to providing structural information about neuroblastoma. With the evolution of MRI technologies, quantitative MRI can not only help assess image-defined risk factors but can also quantitatively reflect the biologic features of neuroblastoma in a noninvasive manner. Therefore, compared with anatomic imaging, these emerging quantitative MRI technologies are expected to provide more imaging biomarkers for the management of neuroblastoma. This review article discusses the current applications of quantitative MRI technologies in evaluating childhood neuroblastoma.

Neuroblastoma is a common childhood solid tumor that primarily occurs in the peripheral sympathetic nerve chain, especially in the adrenal and retroperitoneal paravertebral regions. It accounts for a substantial proportion of pediatric cancer cases. Originating from neural crest cells, neuroblastoma presents diverse clinical manifestations, ranging from localized growths that can be surgically resected to widespread metastatic disease (1). Given the highly variable prognosis of patients with neuroblastoma, it is crucial to develop advanced diagnostic and prognostic tools to guide effective treatment strategies.

MRI has emerged as an important imaging modality in the management of neuroblastoma. Unlike CT, MRI offers the advantage of being free from ionizing radiation, making it particularly suitable for repeated use in pediatric patients. By utilizing MRI, radiologists can determine the anatomic relationship between neuroblastoma and adjacent structures, thereby providing critical guidance for the surgical resection and treatment response evaluation of neuroblastoma (2). However, although anatomic imaging can provide some quantitative information, such as percentage change in tumor size and attenuation measurements, as well as qualitative information about the morphology and structure of neuroblastoma, it is insufficient for prognostic evaluation of the disease. A previous study indicated that percentage change in tumor size was not a predictor of high-risk neuroblastoma prognosis (3).

Quantitative MRI techniques, such as multi-*b*-value diffusion-weighted imaging (DWI) and amide proton transfer-weighted (APTw) imaging, can not only present the morphologic and structural characteristics of lesions but can also provide insights into the biologic features of tumors beyond anatomic visualization, in a noninvasive manner (4). By applying these emerging quantitative MRI techniques, we can identify more imaging biomarkers associated with the prognosis of neuroblastoma, thereby facilitating the development of personalized medicine for these patients. For example, a previous study found that a low baseline apparent diffusion coefficient (ADC) value was associated with tumor progression and relapse in patients with neuroblastoma (5). This review discusses the current applications of quantitative MRI technologies in evaluating childhood neuroblastoma (Table 1).

Epidemiology and Pathophysiology of Neuroblastoma

Neuroblastoma is the most frequently diagnosed malignancy during infancy, accounting for about 8%–10% of all childhood cancers. A report from the Netherlands indicated that 45% of the 593 newly diagnosed neuroblastoma cases between 1990 and 2014 were in children younger than 18 months of age, and 52% had stage IV disease (6). The overall age-adjusted incidence rate of neuroblastoma in Southeast Europe registries between 1990 and 2016 was 10.1 per million persons (7). A comprehensive analysis of neuroblastoma incidence in the United States between 2001 and 2019 revealed that the age-adjusted incidence of 11 543 primary neuroblastoma cases was 8.3 per million persons, with an average annual percent change of 0.4% (8).

Neuroblastoma originates from neural crest cells, which are embryonic cells that normally develop into the peripheral sympathetic nervous system. This tumor can occur anywhere along the sympathetic chain from the neck to the pelvis (Fig 1), particularly in the adrenal gland and paraspinal ganglia, and occasionally occurs in the central nervous system. Neuroblastoma frequently metastasizes to the bone, bone marrow, liver, lymph nodes, and skin. Metastasis can be either single- or multiple-site. Liu et al (9) found that bone was the most common site of metastasis (42.6%), followed by the liver (10.9%), lung (1.3%), and brain (0.2%), among patients with single-organ metastasis. They also found that the combination of bone and liver metastases was the most common form of multiple-site metastasis, accounting for 9.5% of cases.

Genetic and molecular abnormalities in neuroblastoma include *MYCN* amplification, chromosomal alterations, and

Abbreviations

ADC = apparent diffusion coefficient, APTw = amide proton transfer-weighted, ASL = arterial spin labeling, AUC = area under the receiver operating characteristic curve, CEST = chemical exchange saturation transfer, DKI = diffusion kurtosis imaging, DWI = diffusion-weighted imaging, DWIBS = DWI with background body signal suppression, IDRF = image-defined risk factor, IVIM = intravoxel incoherent motion, MIBG = metaiodobenzylguanidine, MRS = MR spectroscopy

Summary

Compared with anatomic imaging, quantitative MRI offers the potential to provide more imaging biomarkers for the diagnosis, risk stratification, treatment response evaluation, and prognosis prediction of childhood neuroblastoma.

Essentials

- Image-defined risk factors derived from anatomic imaging of neuroblastoma are limited to providing only structural information about the tumor.
- Quantitative MRI demonstrates the ability to help predict prognosis, including overall survival, in patients with neuroblastoma and may provide more imaging biomarkers compared with anatomic imaging.
- Quantitative MRI-derived indicators and image-defined risk factors could serve as complementary biomarkers for neuroblastoma.

Keywords

Pediatrics, MR–Functional Imaging, Children, MRI, Neuroblastoma, Quantitative Imaging

mutations in the *ALK* gene. While most neuroblastoma cases are sporadic, approximately 1%–2% are familial. Familial cases are often associated with mutations in the *PHOX2B* and *ALK* genes (10).

Staging and Treatment of Neuroblastoma

Due to the heterogeneity of neuroblastoma, patient prognosis varies widely. The overall survival rate for low-risk patients can exceed 90% but remains around 50% for high-risk patients (11). Therefore, to improve the prognosis and quality of life for patients with neuroblastoma, it is essential to perform risk stratification and implement tailored treatment strategies for each risk group. Over the past 15 years, the International Neuroblastoma Risk Group has developed an imaging-based staging system to stratify neuroblastoma preoperatively (12). This system introduced 20 image-defined risk factors (IDRFs) (Table 2) to stage neuroblastoma into L1, L2, M, and MS stages (Table 3, Fig 2). These IDRFs, combined with clinical features, are used to classify patients into very-low-, low-, intermediate-, and high-risk groups (13).

The treatment of neuroblastoma varies across different risk groups. For low-risk patients, particularly those without IDRFs, upfront surgery can completely remove the primary tumor in most cases. Conversely, high-risk patients require a combined treatment approach that includes surgical removal, induction and postoperative chemotherapy, radiation therapy, and hematopoietic stem cell transplantation (14). Additionally, immunotherapy with anti-GD2 monoclonal antibodies is beneficial for high-risk patients (15). Due to the propensity of neuroblastoma to encase vascular structures and invade adjacent organs, upfront surgical removal is typically not performed for intermediate- and high-risk patients. Instead, induction chemotherapy is used to shrink the tumor before surgery.

Role of Anatomic Imaging in Neuroblastoma

Anatomic imaging can be used to determine tumor size and identify IDRFs in neuroblastoma (Fig 3), which helps guide surgical resection. As mentioned earlier, the identification of IDRFs is integral to neuroblastoma staging, which helps assess disease extent and stratify risk. The IDRF-based staging system has been widely validated in the management of neuroblastoma, regardless of surgical resection or prognosis evaluation (16,17). For surgeons, detailed anatomic imaging is crucial for planning tumor resection approaches. In cases without IDRFs, laparoscopic surgery can be performed safely and effectively, as noted in a previous study (18). Zenitani et al (19) have also found that laparoscopic resection of abdominal neuroblastoma in children is a feasible and safe procedure for tumors less than 60 mm in diameter without IDRFs. Additionally, identifying IDRFs can help predict surgical complications in neuroblastoma (20).

Similarly, anatomic imaging can also help evaluate treatment response in neuroblastoma. Some studies have found that induction chemotherapy helps reduce the number of IDRFs in neuroblastoma, although some vascular-related IDRFs respond less effectively to this treatment (21). In induction chemotherapy, assessing tumor size is helpful for evaluating the primary site treatment response. Previously, the International Neuroblastoma Response Criteria often used the ellipsoid formula to calculate tumor volume. However, Bagatell et al (3) have shown that there is no evidence of a difference in prognosis prediction between using the ellipsoid formula and the single longest dimension to assess treatment response in high-risk neuroblastoma. Therefore, the latest revised International Neuroblastoma Response Criteria have adopted the single longest dimension to evaluate treatment response at the primary site (22). For the primary tumor, a complete response is defined as the presence of less than 10 mm of residual soft tissue at the primary site and complete resolution of metaiodobenzylguanidine (MIBG) or fluorodeoxyglucose PET uptake (for MIBG-nonavid tumors) at the primary site. A partial response for the primary tumor is defined as a decrease of 30% or more in the longest diameter of the primary site, along with MIBG or fluorodeoxyglucose PET uptake at the primary site that is stable, improved, or resolved.

Limitations of Anatomic Imaging in Neuroblastoma

Although anatomic imaging is validated for neuroblastoma surgical planning, it remains inadequate for prognostic evaluation of the disease, especially in high-risk neuroblastoma. A previous study showed that changes in tumor size do not predict high-risk neuroblastoma prognosis (3). Additionally, the role of primary tumor resection in high-risk neuroblastoma remains controversial. Yeung et al (23) found no evidence of differences in terms of 5-year event-free survival and overall survival among the complete gross tumor resection, gross total resection, and subtotal tumor resection groups in high-risk stage IV neuroblastoma.

When investigating the ability of pretreatment IDRFs to predict *MYCN* amplification and overall survival in neuroblastoma, a previous study reported area under the receiver operating characteristic curve (AUC) values of 0.74 and 0.70, respectively,

Table 1: Summary of Principles and Current Applications of Quantitative MRI Techniques in Neuroblastoma

Technique	How It Works	Application	Limitation
DWI	Measures water molecule diffusion differences	Pathologic correlation: neuroblastoma, ganglioneuroblastoma, ganglioneuroma (26–29) Genetic relevance: *MYCN* amplification (30,31) Differential diagnosis: neuroblastoma and Wilms tumor (32,33) Chemotherapy and prognosis evaluation (5,30,34,35) Distant metastasis detection (36) Skeletal scoring (37)	Uses a monoexponential model and can be influenced by microcirculation and blood perfusion
DKI	Captures non-Gaussian diffusion for tissue complexity	Differential diagnosis: olfactory neuroblastoma and nasal squamous cell carcinoma (40)	Requires ultra-high *b* values; prone to artifacts and lacks standardized *b* values
MRS	Measures the difference in the resonance frequency of specific atomic nuclei in a magnetic field to analyze	Differential diagnosis (42) Genetic relevance (43) Chemotherapy evaluation (44)	Long acquisition time, motion sensitive, complex data processing
IVIM	Uses biexponential model for diffusion measurement	Differential diagnosis: neuroblastoma and Wilms tumor (32)	Assumes Gaussian water diffusion, not suitable for heterogeneous tumors
ASL MRI	Uses radiofrequency pulses to measure arterial blood flow	Perfusion measurements (47)	Technically complex, motion sensitive, long acquisition, low spatial resolution
APTw imaging	Detects chemical exchange saturation transfer signals associated with proteins and polypeptides	Pathologic correlation (51) Risk stratification (4,52)	Motion artifacts, magnetic field sensitivity, unclear signal sources
Native T1 mapping	Measures longitudinal relaxation time of tissues at different recovery time points	Pathologic correlation (53) Treatment evaluation (53)	Variable scan time, dependent on sequence, limited validation in neuroblastoma

Note.—APTw = amide proton transfer-weighted, ASL = arterial spin labeling, DKI = diffusion kurtosis imaging, DWI = diffusion-weighted imaging, IVIM = intravoxel incoherent motion, MRS = MR spectroscopy.

indicating only moderate diagnostic performance (17). These results suggest that anatomic imaging alone is insufficient to effectively predict the prognosis of neuroblastoma.

Another investigation suggested that anti-GD2 immunotherapy can reduce the number of IDRFs in neuroblastoma; however, there was no evidence of a difference in the reduction of IDRFs between the groups receiving immunotherapy and those not receiving it (24). Furthermore, routine imaging examinations cannot effectively detect the treatment response of high-risk neuroblastoma to anti-GD2 immunotherapy, highlighting certain limitations of these imaging methods (25). In this clinical context, the emerging quantitative MRI technologies are expected to provide more quantitative imaging biomarkers, improving the ability to stratify neuroblastoma risk and predict prognosis (Table 4).

DWI in Neuroblastoma

Pathologic Correlation

DWI can track the Brownian motion of water molecules within tissues at a microscopic level. One of the important indicators of DWI is ADC, which quantitatively reflects the microstructural status of cellular tissues. Neuroblastoma, due to its high nuclear-cytoplasmic ratio and dense arrangement of tumor cells, restricts the movement of water molecules (26). This leads to elevated signal intensity of neuroblastoma at a high *b* value at DWI compared with tissues with free diffusion of water. This restricted diffusion corresponds to a low ADC value. However, ADC values vary among different histopathologic subtypes of neuroblastic tumors and exhibit an increasing trend in neuroblastoma, ganglioneuroblastoma, and ganglioneuroma (27). Wen et al (28) explored the value of DWI in evaluating the degree of tumor cell differentiation in patients with ganglioneuroblastoma-nodular and ganglioneuroblastoma-intermixed subtypes. The results showed that the ADC values of ganglioneuroblastoma-nodular were lower than those of ganglioneuroblastoma-intermixed. These imaging findings could be explained by the fact that ganglioneuroblastoma-nodular is more malignant than ganglioneuroblastoma-intermixed, and the mitosis-karyorrhexis index in the former is also higher than that in the latter. Additionally, the authors found that the ADC values of undifferentiated or poorly differentiated neuroblastoma were lower than those of their differentiated counterparts. Therefore, DWI can be helpful for the noninvasive assessment and initial evaluation of childhood neuroblastic tumors (29).

Genetic Relevance

In addition to providing pathologic information, DWI quantitative indicators can be used as imaging biomarkers for revealing the genetic characteristics of neuroblastoma. The *MYCN* onco-

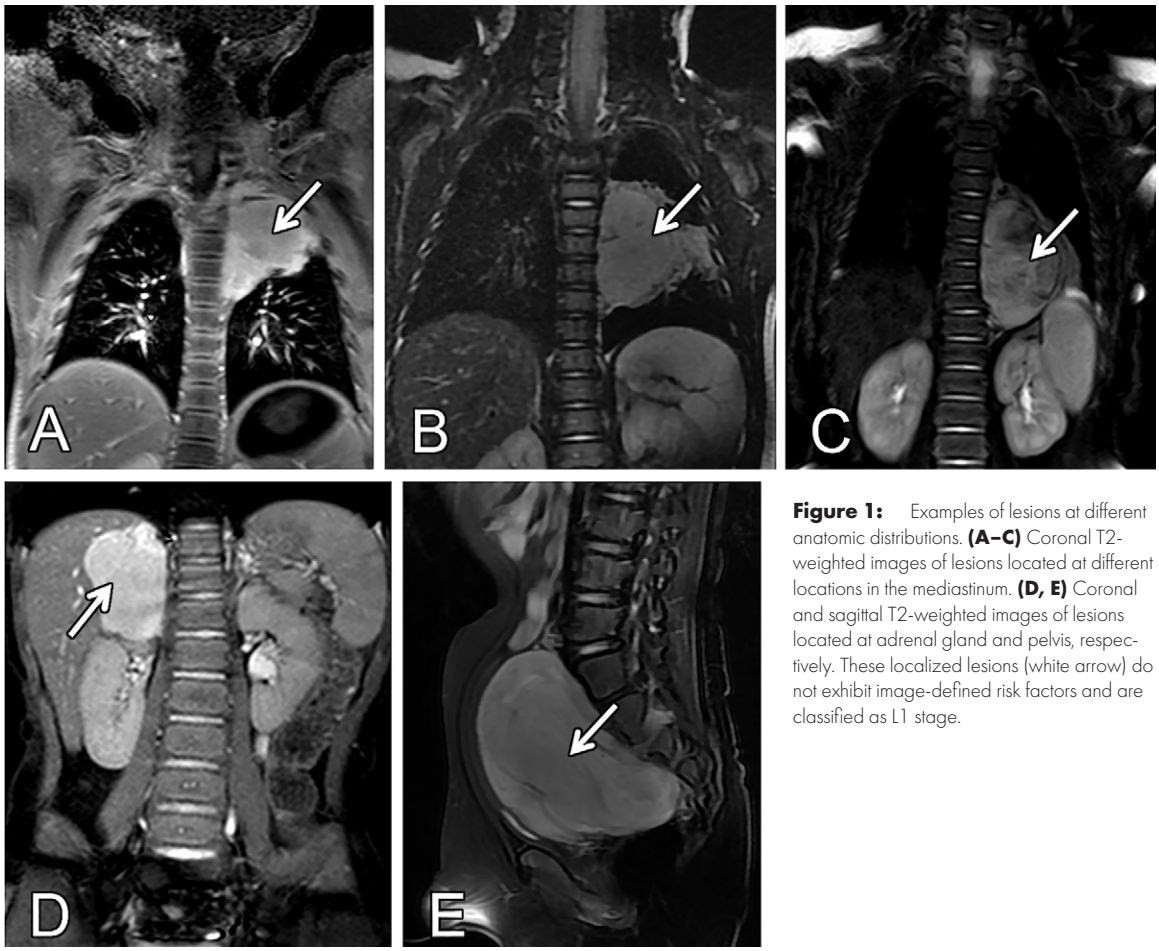

Figure 1: Examples of lesions at different anatomic distributions. **(A–C)** Coronal T2-weighted images of lesions located at different locations in the mediastinum. **(D, E)** Coronal and sagittal T2-weighted images of lesions located at adrenal gland and pelvis, respectively. These localized lesions (white arrow) do not exhibit image-defined risk factors and are classified as L1 stage.

Table 2: Description of Image-defined Risk Factors of Neuroblastoma

Anatomic Site	Definition
Neck-chest, chest-abdomen, abdomen-pelvis	Ipsilateral tumor extension within two body compartments
Neck	Tumor encasing carotid and/or vertebral artery and/or internal jugular vein Tumor extending to base of skull Tumor compressing the trachea
Cervicothoracic junction	Tumor encasing brachial plexus roots Tumor encasing subclavian vessels and/or vertebral and/or carotid artery Tumor compressing the trachea
Thorax	Tumor encasing the aorta and/or major branches Tumor compressing the trachea and/or principal bronchi Lower mediastinal tumor, infiltrating the costovertebral junction between T9 and T12
Thoracoabdominal	Tumor encasing the aorta and/or vena cava
Abdomen or pelvis	Tumor infiltrating the porta hepatis and/or the hepatoduodenal ligament Tumor encasing branches of the superior mesenteric artery at the mesenteric root Tumor encasing the origin of the celiac axis and/or of the superior mesenteric artery Tumor invading one or both renal pedicles Tumor encasing the aorta and/or vena cava Tumor encasing the iliac vessels Pelvic tumor crossing the sciatic notch
Intraspinal tumor extension	More than one-third of the spinal canal in the axial plane is invaded and/or the perimedullary leptomeningeal spaces are not visible and/or the spinal cord signal is abnormal
Infiltration of adjacent organs or structures	Pericardium, diaphragm, kidney, liver, duodenopancreatic block, and mesentery

Source.—Reference 12.

gene is mainly expressed in embryonic tissues and developing nervous tissues, playing an important role in embryonic and nervous system development. Amplification of the *MYCN* oncogene is associated with the occurrence and progression of neuroblastoma, particularly within high-risk subgroups, and correlates with a poor prognosis for patients (10). Neubauer et al (30) found that *MYCN*-amplified neuroblastoma had lower ADC values compared with nonamplified neuroblastoma, and the average signal intensity ratio of the tumor to surrounding tissue was relatively lower in *MYCN*-amplified neuroblastoma. However, these findings require further validation with a larger sample size. By comparing the ADC histogram indicators of *MYCN*-amplified and nonamplified neuroblastoma groups in 62 patients, Ghosh et al (31) found that the maximum ADC value of *MYCN*-amplified neuroblastoma was significantly higher and the minimum ADC value was significantly lower than that of the control group. Additionally, the entropy, variance, energy, and uniformity of the ADC histogram also showed significant statistical differences between *MYCN*-amplified and nonamplified groups. Although there was a significant association between IDRFs and *MYCN* amplification in neuroblastoma, the performance of IDRFs in detecting *MYCN* amplification was moderate (17). Therefore, whether the combination of IDRFs and ADC values can further improve performance for predicting *MYCN* amplification in neuroblastoma is worthy of further study.

Differential Diagnosis

Another potential application of DWI is in the differential diagnosis of neuroblastoma from other pediatric tumors. Aslan et al (32) found that the ADC values of abdominal neuroblastoma were significantly lower than those of Wilms tumor, suggesting that DWI can help distinguish between the two most common retroperitoneal solid tumors in children. In the aforementioned studies, researchers typically selectively delineate the regions of interest of tumors on typical planes and often use mean or minimum ADC values to assess the utility of DWI in the diagnosis and differential diagnosis of neuroblastoma. However, considering the heterogeneity of neuroblastoma, relying solely on selectively delineated regions of interest and a single ADC value may not fully reveal the biologic characteristics of neuroblastoma. Through analysis of the ADC histogram based on whole tumor lesions located in the pediatric abdomen, Meeus et al (33) found that ADC histogram parameters such as kurtosis, skewness, and entropy were significantly higher, while the mean, median, and percentile ADC values were significantly lower in malignant tumors compared with benign tumors. Figure 4 illustrates the DWI-derived parameter maps of a grade IV neuroblastoma. Despite the assistance these histogram parameters provide in distinguishing between benign and malignant abdominal tumors, there are still limitations in their ability to differentiate between other types of malignant tumors such as neuroblastoma and Wilms tumor.

Table 3: International Neuroblastoma Risk Group Staging System

Stage	Definition
L1	Localized tumor without image-defined risk factors
L2	Local-regional tumor with one or more image-defined risk factors
M	Distant metastatic disease (except stage MS)
MS	Metastatic disease in children younger than 18 months with metastases confined to skin, liver, and/or bone marrow

Source.—Reference 13.

Chemotherapy and Prognosis Evaluation

Traditionally, imaging techniques have been used to assess the effect of chemotherapy in neuroblastoma primarily by judging changes in tumor size and volume. In a study evaluating the efficacy of chemotherapy in neuroblastoma using DWI, researchers compared the ADC values of abdominal-pelvic neuroblastoma before and after chemotherapy (34). They found a significant increase in ADC values after chemotherapy. Neubauer et al (30) compared the signal intensity ratio of DWI and contrast-enhanced T1-weighted imaging before and after chemotherapy in neuroblastoma. Although the signal intensity ratio decreased in both modalities, DWI exhibited a greater signal intensity ratio compared with contrast-enhanced T1-weighted imaging, suggesting that DWI not only quantifies the efficacy of chemotherapy in neuroblastoma but also more effectively reflects lesion characteristics. In another study, Privitera et al (35) investigated the correlation between ADC values and MIBG uptake values in high-risk neuroblastoma before and after chemotherapy, and they discovered that the 25th percentile ADC value

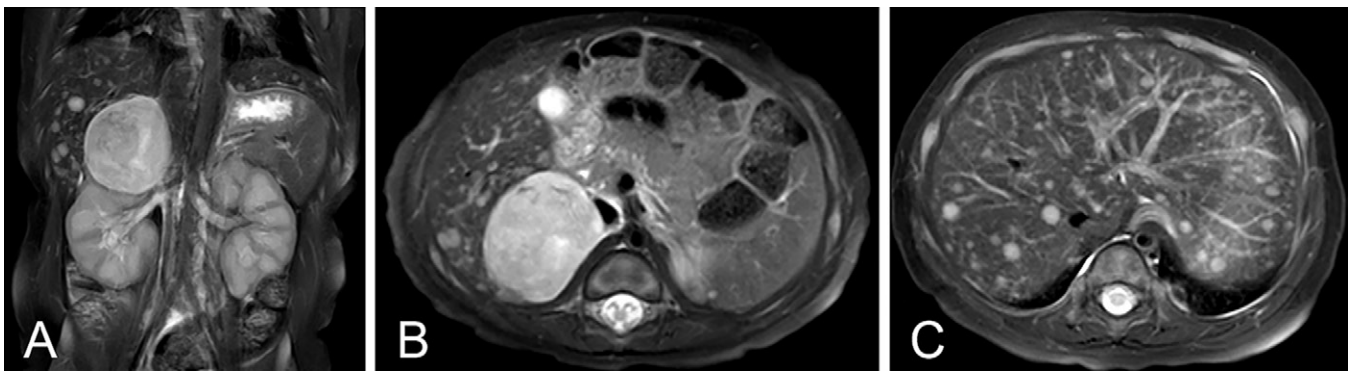

Figure 2: A case of abdominal neuroblastoma in a 1-month-old male infant. **(A)** Coronal and **(B)** axial T2-weighted images indicate that the primary lesion is confined to the right adrenal gland without image-defined risk factors. **(C)** Axial T2-weighted image shows that metastatic lesions are confined to the liver. This case is classified as MS stage.

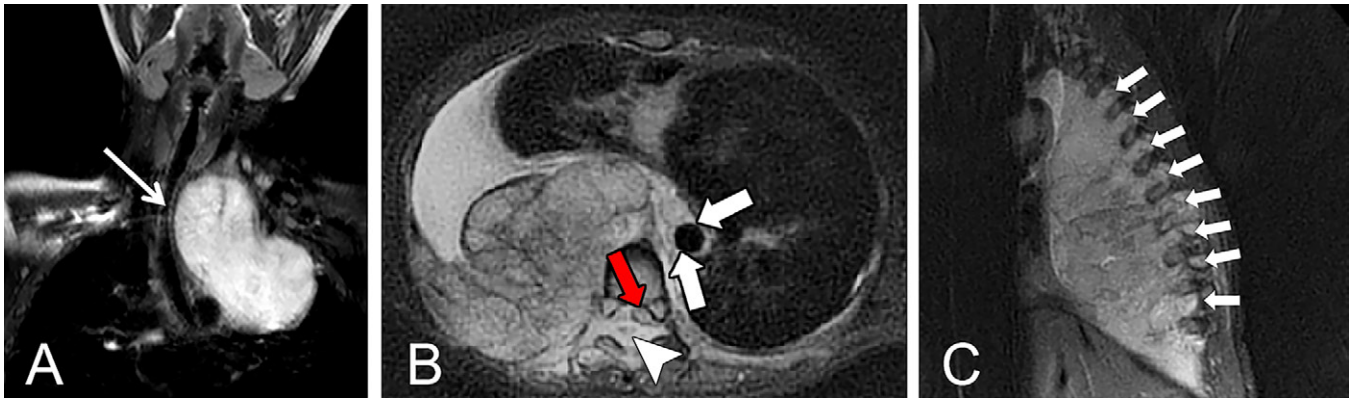

Figure 3: **(A)** Coronal T2-weighted image shows an example of a lesion located at the cervicothoracic junction compressing the trachea (white arrow) in a 36-month-old female child, classified as L2 stage. **(B)** Axial and **(C)** sagittal T2-weighted images show an example of a tumor infiltrating the costovertebral junction and expanding into the vertebral canal in a 26-month-old female child diagnosed with high-risk neuroblastoma located in the thorax. **(B)** Axial T2-weighted image shows the spinal cord (red arrow) compressed to the left by the tumor (white arrowhead). The tumor only contacts the aorta, indicating it envelops less than 50% of the aorta's perimeter (white arrows). **(C)** Sagittal T2-weighted image shows the tumor infiltrating the costovertebral junction between T4 and T12 (white arrows).

Table 4: Summary of Reports Related to Quantitative MRI Techniques in Neuroblastoma Discussed in This Article

Technique and Author	Year	Country	Sample Size	Study Design	Key Findings	Clinical Relevance
DWI						
Uhl et al (26)	2002	Germany	7 neuroblastomas	Prospective, single center	DWI showed an increased tumor signal, which correlated with small cell histology	Provides a histopathologic basis for DWI in neuroblastoma
Gahr et al (27)	2011	Germany	10 neuroblastomas, 2 ganglioneuroblastomas, 4 ganglioneuromas	Prospective, multicenter	The mean ADC for neuroblastoma was significantly lower than that of ganglioneuroblastoma and ganglioneuroma (P = .01)	Differentiates between neuroblastoma and ganglioneuroblastoma and ganglioneuroma
Demir et al (34)	2015	Turkey	11 neuroblastomas, 4 ganglioneuroblastomas	Retrospective, single center	Postchemotherapy ADC was significantly higher than prechemotherapy ADC (P = .003)	Assesses chemotherapy response in neuroblastoma
Serin et al (29)	2016	Turkey	15 neuroblastomas, 5 ganglioneuroblastomas, 4 ganglioneuromas	Retrospective	The mean ADC of neuroblastoma was significantly lower than that of ganglioneuroblastoma and ganglioneuroma (P = .026)	Establishes an ADC cutoff for differentiating neuroblastoma from ganglioneuroblastoma and ganglioneuroma
Aslan et al (32)	2017	Turkey	10 neuroblastomas, 7 Wilms tumors	Retrospective, single center	ADC values were lower in neuroblastoma than in Wilms tumor (P < .05)	Differentiates neuroblastoma from Wilms tumor
Wen et al (28)	2017	China	15 neuroblastomas, 7 ganglioneuroblastomas (nodular = 3; intermixed = 4), 3 ganglioneuromas	Retrospective, single center	ADC values were significantly lower in neuroblastoma than in ganglioneuroblastoma and ganglioneuroma (P < .001)	Correlates ADC values with histologic types and differentiation grades
Neubauer et al (30)	2017	Germany	19 neuroblastomas, 4 ganglioneuroblastomas, 6 ganglioneuromas	Retrospective, single center	ADC values after therapy were significantly higher than before therapy (P < .05)	Aids in evaluating chemotherapy response and differentiating neuroblastic tumors

(Table 4 continues)

Table 4 *(continued)*: Summary of Reports Related to Quantitative MRI Techniques in Neuroblastoma Discussed in This Article

Technique and Author	Year	Country	Sample Size	Study Design	Key Findings	Clinical Relevance
Ishiguchi et al (36)	2018	Japan	12 neuroblastomas	Retrospective, single center	Whole-body DWI had similar sensitivity to fluorine 18 FDG PET/CT for lymph node metastasis detection	Shows potential in detecting bone and lymph node metastases
Meeus et al (33)	2018	United Kingdom	43 patients with abdominal tumors (32 malignant, 10 benign; 11 neuroblastomas, 8 Wilms tumors)	Retrospective, single center	ADC values were significantly lower in malignant tumors compared with benign ($P < .05$)	Differentiates malignant pediatric abdominal tumors from benign ones
Peschmann et al (5)	2019	Germany	15 neuroblastomas, 1 ganglioneuroblastoma, 3 ganglioneuromas	Retrospective, single center	The initial ADC of neuroblastoma with eventual tumor relapse was less than 0.80 × 10^{-3} mm^2/sec	Highlights the prognostic value of ADC values in neuroblastoma
Privitera et al (35)	2021	United Kingdom	40 neuroblastomas	Retrospective, single center	Tumors that showed greater shrinkage had lower pretreatment tumor ADC25prc values ($P < .001$)	Complements iodine 123–MIBG avidity as biomarkers for chemotherapy response
Gassenmaier et al (37)	2021	Germany	17 neuroblastomas	Retrospective, single center	Whole-body MRI had higher scores than MIBG scintigraphy ($P = .018$)	Offers more detailed scoring for neuroblastoma assessment
Ghosh et al (31)	2022	United States	62 neuroblastomas	Retrospective, single center	*MYCN*-amplified neuroblastomas had significantly higher ADC metrics than nonamplified ones ($P < .05$)	Establishes correlation between ADC values and *MYCN* amplification in neuroblastoma
IVIM						
Meeus et al (33)	2018	United Kingdom	43 patients with abdominal tumors (32 malignant, 10 benign; 11 neuroblastomas, 8 Wilms tumors)	Retrospective, single center	D^* and f were higher in neuroblastoma than Wilms tumors ($P < .05$)	Differentiates neuroblastoma from Wilms tumor
DKI						
Xiao et al (40)	2018	China	17 olfactory neuroblastomas, 23 squamous cell carcinomas	Retrospective, single center	Kurtosis values were significantly higher in olfactory neuroblastomas than squamous cell carcinomas ($P < .001$)	Highlights the potential value of DKI for neuroblastoma
MRS						
Lindskog et al (44)	2004	Sweden	NA	Experimental	Methylene to choline ratio correlates with tumor regression in chemotherapy	Predicts chemotherapy response in neuroblastoma
Peet et al (43)	2007	United Kingdom	NA	Experimental	*MYCN*-amplified cell lines had higher phosphocholine levels than nonamplified lines ($P < .05$)	Identifies metabolic differences in *MYCN*-amplified neuroblastoma

(Table 4 continues)

Table 4 *(continued)*: Summary of Reports Related to Quantitative MRI Techniques in Neuroblastoma Discussed in This Article

Technique and Author	Year	Country	Sample Size	Study Design	Key Findings	Clinical Relevance
Kohe et al (42)	2018	United Kingdom	70 neuroblastomas, 50 retinoblastomas, 39 medulloblastomas	Retrospective, in vitro	Significant differences in metabolite concentrations were found among tumor types ($P < .0017$)	Identifying metabolic differences to differentiate neuroblastoma
ASL MRI						
Harteveld et al (47)	2022	The Netherlands	4 neuroblastomas, 6 nephroblastomas	Retrospective, single center	Tumors exhibited low perfusion-weighted signals compared with kidneys	Assesses perfusion in pediatric abdominal tumors
APTw imaging						
Tanoue et al (51)	2019	Japan	NA	Experimental	The neuroblastoma model showed a significantly higher magnetization transfer ratio asymmetry than the breast cancer model	Assesses proliferative potential in neuroblastoma
Jia et al (52)	2022	China	24 neuroblastomas, 18 Wilms tumors, 15 hepatoblastomas	Prospective, single center	APTw imaging signals were significantly higher in high-risk neuroblastomas ($P < .001$)	Aids in neuroblastoma risk stratification
Jia et al (4)	2023	China	34 neuroblastomas	Prospective, single center	APTw values were higher in high-risk neuroblastomas compared with non-high-risk ones ($P < .001$)	Differentiates high-risk from non-high-risk neuroblastomas
Native T1 mapping						
Zormpas-Petridis et al (53)	2020	United Kingdom	NA	Experimental	High native T1 regions correlated with proliferative neuroblasts	Aids in assessing histopathologic heterogeneity and therapy response in neuroblastoma

Note.—ADC = apparent diffusion coefficient, ADC25prc = lower quartile ADC value, APTw = amide proton transfer-weighted, ASL = arterial spin labeling, DKI = diffusion kurtosis imaging, DWI = diffusion weighted imaging, FDG = fluorodeoxyglucose, IVIM = intravoxel incoherent motion, MIBG = metaiodobenzylguanidine, MRS = MR spectroscopy, NA = not applicable.

after chemotherapy accurately identified areas of inactive tumor cells. Figure 5 shows the correlation between ADC map features and iodine 123–MIBG uptake after chemotherapy for high-risk neuroblastoma. These findings suggest that calculating ADC values of neuroblastoma after chemotherapy can aid in providing guidance for surgical resection.

In terms of prognosis prediction, Peschmann et al (5) found that lower baseline ADC values were associated with malignant progression and recurrence of the neuroblastoma through comparison of tumor ADC values at initial presentation and at 3-month follow-up. Additionally, during the course of treatment, there was a correlation between ADC values and patients' event-free survival, with a decrease in ADC values being an indicator of poor prognosis. This indicates the potential of ADC values to predict patient prognosis. Figure 6 shows baseline MR images of nonrelapsing neuroblastoma. These reports suggest that DWI quantitative indicators provide potential support in assessing the treatment response and prognosis of patients with neuroblastoma.

Distant Metastasis Detection and Skeletal Scoring

In the quantitative analysis of neuroblastoma, DWI exhibits a level of performance comparable to nuclear medicine imaging techniques and can serve as a complementary imaging biomarker. Whole-body DWI with background body signal suppression (DWIBS) can reduce the visibility of nonrelevant background signals, allowing for clearer visualization of lesions by minimizing interference from surrounding tissues. Compared with PET imaging, DWIBS demonstrates similar sensitivity but lower specificity and overall accuracy in helping detect bone and lymph node metastases (36). For skeletal scoring of high-risk neuroblastoma, the use of radiolabeled MIBG has prognostic value and can be used for risk stratification of neuroblastoma.

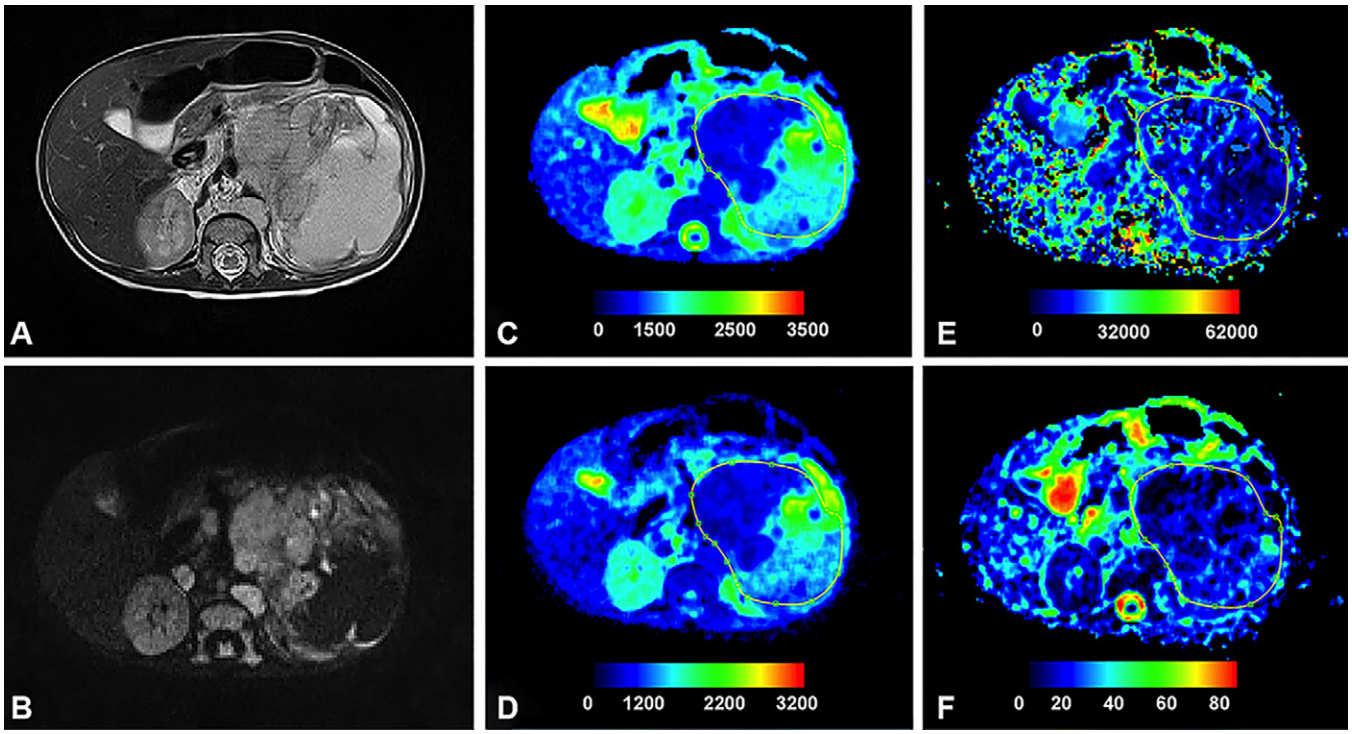

Figure 4: A case of grade IV neuroblastoma. **(A, B)** Axial T2-weighted and *b* value of 150 sec/mm² images, respectively. **(C–F)** Maps for the apparent diffusion coefficient, *D*, *D**, and *f*, respectively. The median values calculated for the apparent diffusion coefficient, *D*, *D**, and *f* from the entire tumor region of interest were 1155 × 10^{-6} mm²/sec, 703 × 10^{-6} mm²/sec, 17762 × 10^{-6} mm²/sec, and 23%, respectively. (Adapted, under a CC BY 4.0 license, from reference 33.)

Through investigating the correlation between MIBG skeletal scoring and whole-body DWI quantitative analysis, Gassenmaier et al (37) found that the International Society of Pediatric Oncology European Neuroblastoma Research Network skeletal scoring system was equally applicable to whole-body MRI compared with MIBG scintigraphy; however, whole-body MRI could result in slightly higher skeletal scores, potentially due to its higher spatial resolution.

Intravoxel Incoherent Motion and Diffusion Kurtosis Imaging in Neuroblastoma

Although DWI based on a monoexponential model can quantitatively assess the movement of water molecules within microstructures, it can be influenced by microcirculation blood perfusion and cannot fully exploit the abundant data information extracted from DWI. In contrast, intravoxel incoherent motion DWI (IVIM-DWI) based on a biexponential model calculates the true diffusion coefficient, pseudodiffusion coefficient, and perfusion fraction using different *b* values, which can more accurately reflect the diffusion and perfusion status within tissues and thus compensate for the shortcomings of conventional DWI (38). Although the application of IVIM-DWI has been reported in adult diseases, investigation on its use in childhood neuroblastoma is relatively limited. Meeus et al (33) indicated that the pseudodiffusion coefficient and perfusion fraction of neuroblastoma were significantly higher than those of Wilms tumor. This difference may stem from the tendency of neuroblastoma to encase surrounding blood vessels, leading to increased microcirculation perfusion within the tumor tissue. Additionally, histogram-derived parameters of pseudodiffusion coefficient and perfusion fraction (such as skewness, kurtosis, and entropy) were also helpful in distinguishing between neuroblastoma and Wilms tumor. Specifically, the skewness of pseudodiffusion coefficient distribution was higher in Wilms tumor, while the kurtosis and entropy of perfusion fraction value distribution were relatively higher in neuroblastoma, possibly related to the heterogeneity and irregularity of vascularization within neuroblastoma.

Conventional DWI assumes that water molecules diffuse according to a Gaussian distribution, and with increasing *b* values, the DWI signal exhibits a monoexponential decay. However, due to the substantial heterogeneity of tumor tissue, the diffusion of water molecules does not follow a simple Gaussian distribution (39). Therefore, diffusion kurtosis imaging (DKI) has been proposed based on non-Gaussian diffusion of water molecules. In DKI, the key measurement indicators usually include kurtosis and diffusion coefficient. Although the application of DKI has not been reported in pediatric thoracoabdominal neuroblastoma, it has been demonstrated to be significantly correlated with histopathologic characteristics in olfactory neuroblastoma. Xiao et al (40) found that the kurtosis of olfactory neuroblastoma was significantly higher than that of nasal squamous cell carcinoma, based on DKI. The AUC and accuracy of the kurtosis for distinguishing between these two tumors were 0.87 and 80%, respectively. Future investigations are needed to further explore whether IVIM-DWI and DKI can provide additional clinical value for the diagnosis and risk stratification of neuroblastoma compared with conventional DWI.

MR Spectroscopy in Neuroblastoma

MR spectroscopy (MRS) utilizes the spin properties of specific atomic nuclei (such as hydrogen 1 [^{1}H], phosphorus 31, carbon 13, and fluorine 19) to noninvasively quantify the metabolite content within tissues. In comparison to traditional anatomic

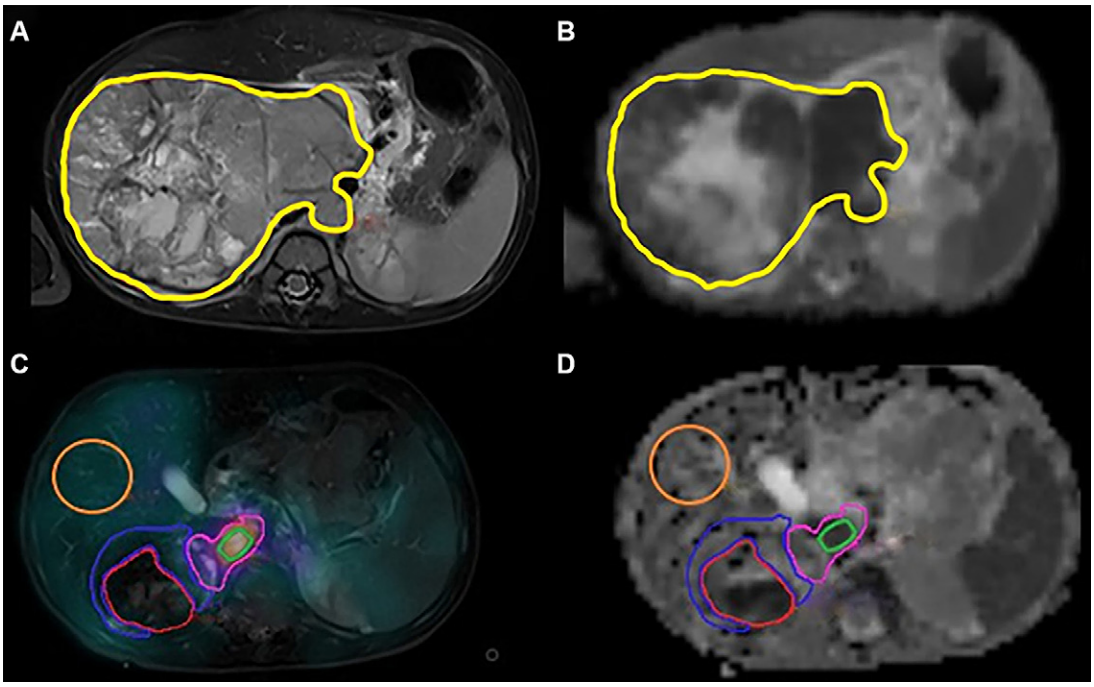

Figure 5: Images in a 20-month-old male patient with high-risk neuroblastoma before and after chemotherapy. **(A, B)** Axial T2-weighted image and apparent diffusion coefficient map of the primary tumor (outlined in yellow) before chemotherapy, respectively. **(C, D)** Axial T2-weighted image and axial apparent diffusion coefficient map registered with SPECT iodine 123 metaiodobenzylguanidine (^{123}I-mIBG) after chemotherapy, respectively. The orange liver region of interest was used for normalization, while different regions of interest within the tumor indicate varying levels of ^{123}I-mIBG uptake. The green, pink, blue, and red regions of interest represent high uptake, moderate uptake, low uptake, and no uptake, respectively. (Adapted, under a CC BY 4.0 license, from reference 35.)

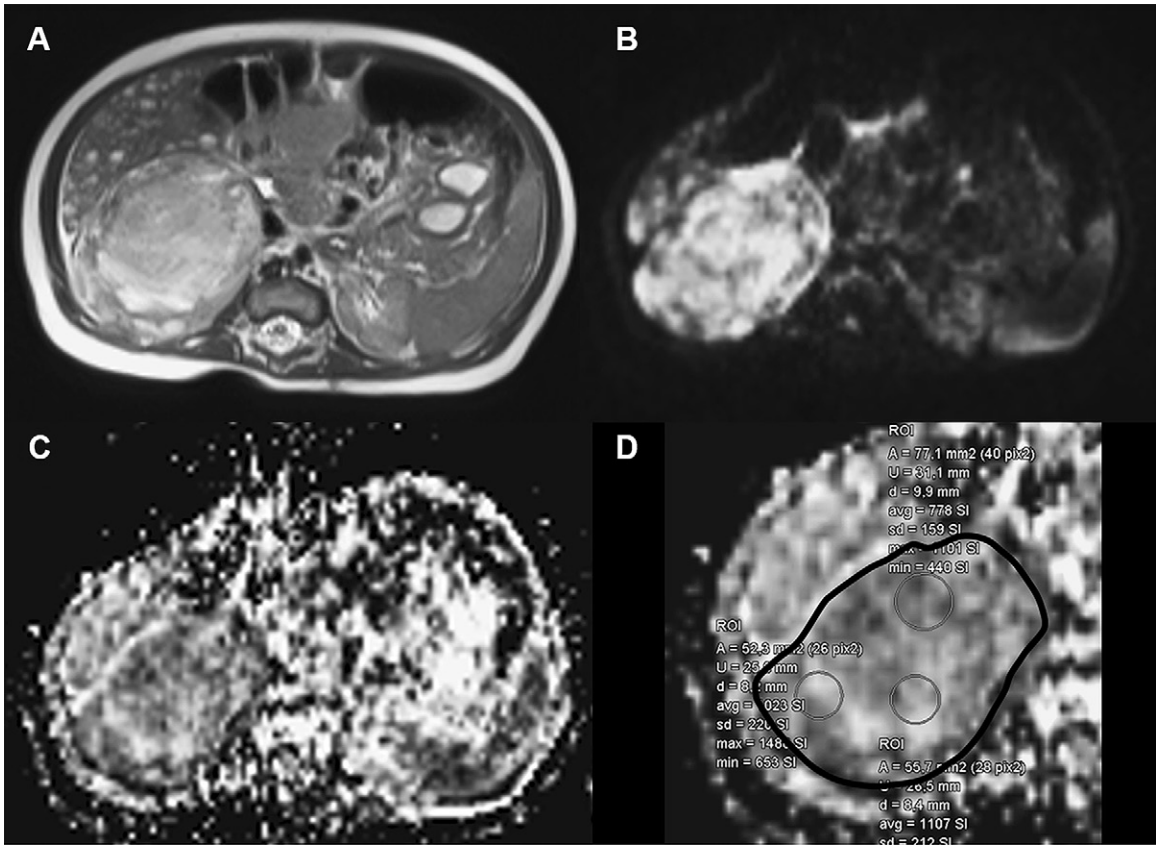

Figure 6: Images of a nonrelapsing neuroblastoma lesion in a 5-week-old male infant. The images include **(A)** a baseline axial T2-weighted image, **(B)** an axial diffusion-weighted image with *b* value of 800 sec/mm^2 , and **(C)** an axial apparent diffusion coefficient map. The baseline apparent diffusion coefficient from the large region of interest was 0.883 × 10^{-3} mm^2/sec. **(D)** Locally enlarged image of **C** shows the different delineated regions of interest (ROIs) for measuring apparent diffusion coefficient values. (Adapted, under a CC BY 4.0 license, from reference 5.)

imaging, MRS enables early and quantitative analysis of metabolic changes in lesions during biochemical processes, such as amino acids, lipids, lactate, and so forth, before morphologic changes occur (41). It holds potential applications in tumor diagnosis and differential diagnosis, early monitoring of treatment response, assessment of tumor cell activity, and identification of potential biomarkers. ^{1}H-MRS has been widely used in both adult and pediatric tumors, particularly in brain, breast, and prostate tumors.

Due to its sensitivity to motion artifacts, MRS is less commonly used in pediatric extracranial tumors such as neuroblastoma. An investigation conducted by Kohe et al (42) suggested that neuroblastoma exhibited higher levels of myoinositol and glutamate-glutamine ratio, indicating metabolic differences in embryonic tumors located outside the central nervous system. Additionally, Peet et al (43) found that neuroblastoma cell lines with *MYCN* amplification showed significantly elevated phosphocholine to total choline and taurine to total choline ratios, while glycerophosphocholine to total choline ratio decreased significantly, suggesting the potential value of MRS metabolite analysis in identifying *MYCN* amplification status. Although an animal experiment showed that ^{1}H-MRS could predict the response or resistance of neuroblastoma to standard chemotherapeutic agents such as platinum-based drugs (44), the clinical utility of MRS in neuroblastoma still requires further research and validation.

Arterial Spin Labeling Imaging in Neuroblastoma

Arterial spin labeling (ASL) imaging can noninvasively assess tissue perfusion by measuring tissue blood flow without the need for injection of contrast agents. Because gadolinium-based contrast agents have the potential risk of causing brain deposition in pediatric patients, and a previous study shows that contrast-enhanced MRI does not provide additional diagnostic value for identifying IDRFs in neuroblastoma (45), the application of contrast-enhanced MRI in pediatric neuroblastoma requires further research and more evidence. Compared with contrast-enhanced MRI using gadolinium-based contrast agents, ASL MRI does not require exogenous contrast agents. The basic principle of ASL MRI involves utilizing the MR pulse to label the spin state in arterial blood flow to obtain a labeled image. Subsequently, this labeled image is subtracted from the unlabeled control image to acquire a perfusion-weighted difference image, thereby enabling the measurement of perfusion parameters (46).

Harteveld et al (47) explored the feasibility of using multidelay pseudocontinuous ASL MRI in pediatric patients with common abdominal solid tumors. They found that the perfusion-weighted signals of neuroblastoma and Wilms tumor were lower than those of the kidneys, and there were differences in perfusion-weighted signals within different regions of the tumors. Figure 7 illustrates the correlation between high intratumoral signal intensity on perfusion-weighted images and low intratumoral signal intensity on T2-weighted images. Additionally, the authors compared ASL MRI with contrast-enhanced T1-weighted imaging and found that the perfusion-weighted signals within the tumors correlated with the degree of enhancement with gadolinium-based contrast agents. This suggests that ASL MRI may assist in noninvasive perfusion measurements of pediatric abdominal solid tumors without introducing gadolinium-based contrast agents. A previous study demonstrated that improved tumor perfusion can enhance drug uptake in neuroblastoma, thereby improving treatment efficacy and reducing the likelihood of systemic toxicity from chemotherapy drugs (48). Therefore, ASL MRI may help monitor changes in blood flow perfusion within neuroblastoma to determine the optimal timing for treatment.

APTw Imaging in Neuroblastoma

APTw imaging is a common technique of chemical exchange saturation transfer (CEST) imaging. CEST is a relatively new molecular imaging technique used to measure chemical exchange between endogenous molecules and water protons. Although the proton resonance frequencies of these endogenous molecules differ from those of water molecules, their proton content is relatively low, making them difficult to be detected directly in conventional MRI. CEST imaging indirectly helps detect the presence of these molecules by suppressing water proton signals and enhancing endogenous molecule proton signals (49). APTw imaging describes the distribution and metabolic information of biologic molecules by exploiting the chemical shift of protons in amide compounds. In APTw imaging, the excitation of protons in amide compounds is first performed using MRI techniques, and then the distribution and concentration of amide compounds in tissues can be inferred by observing changes in signal intensity at different chemical shifts (50). Therefore, APTw imaging holds potential applications in tumor imaging and could aid in the diagnosis and treatment monitoring of tumors.

APTw imaging indicators have been shown to correlate with the pathologic characteristics and risk stratification of neuroblastoma. In an animal experiment, Tanoue et al (51) found that APTw imaging effects not only reflect the proliferative potential of tumor cells in neuroblastoma but also indicate the presence of hemorrhage within the tumor. Jia et al (52) analyzed 57 cases of common solid tumors in the pediatric abdomen, including neuroblastoma, hepatoblastoma, and Wilms tumor, and analyzed the differences in APTw imaging quantitative indicators among different risk groups. They found significant statistical differences in APTw imaging quantitative indicators between high-risk neuroblastoma and low-risk neuroblastoma, but not in hepatoblastoma and Wilms tumor. The AUC for distinguishing low-risk neuroblastoma and high-risk neuroblastoma based on APTw imaging quantitative indicators reached 0.93. Figure 8 shows that neuroblastoma lesions in different risk groups have different APTw imaging signals, with the intermediate-risk and high-risk lesions displaying higher APTw imaging signals. Although neuron-specific enolase has clinical diagnostic value for neuroblastoma, the study by Jia et al (4) showed that there was no evidence of a difference in neuron-specific enolase between high-risk neuroblastoma and non–high-risk neuroblastoma; however, APTw imaging quantitative indicators showed significant value in neuroblastoma risk stratification. Given the potential for more IDRFs in high-risk neuroblastoma, the comparison between anatomic imaging and APTw imaging for differentiating high-risk from non–high-risk neuroblastoma remains a valuable area for future exploration.

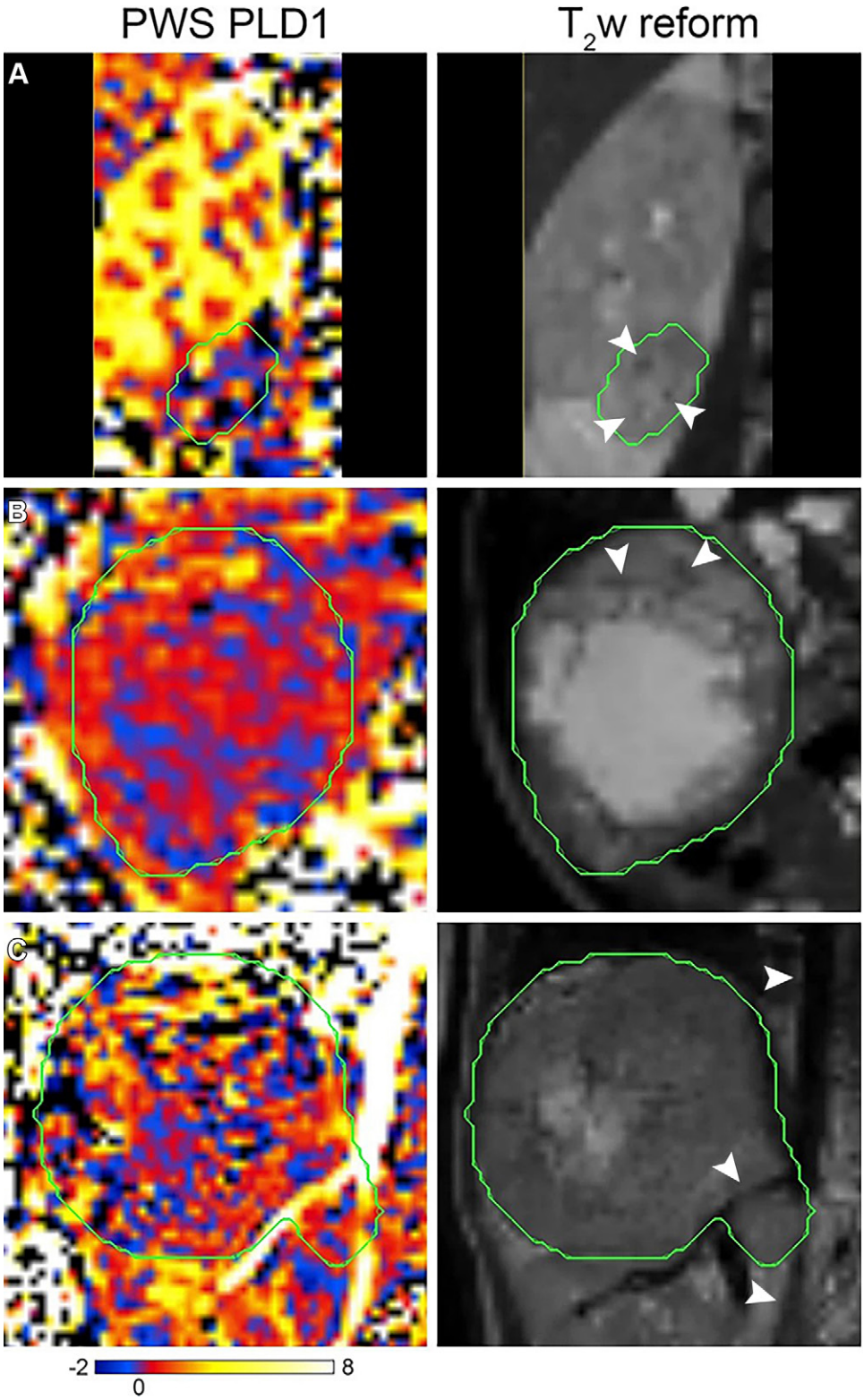

Figure 7: **(A, B)** Perfusion-weighted signal (PWS) and T2-weighted (T2W) images in an 8.3-year-old female patient and a 2.2-year-old female patient, respectively, with Wilms tumor. The images show that the high perfusion-weighted signal areas within the tumor correspond to the low signal intensity areas on the T2-weighted image (white arrowheads). **(C)** Perfusion-weighted signal and T2-weighted images in a 3.8-year-old male patient with neuroblastoma shows that the marked high-signal descending aorta and right renal artery on the perfusion-weighted signal image correspond to the regions on the T2-weighted image (white arrowheads). (Adapted, under a CC BY 4.0 license, from reference 47.)

Native T1 Mapping in Neuroblastoma

Native T1 mapping is used to measure tissue T1 relaxation time, which is the time required for a substance to return to its equilibrium after being stimulated by a pulse signal. Because different tissues have distinct T1 relaxation times, native T1 mapping can quantitatively characterize tissue properties. During

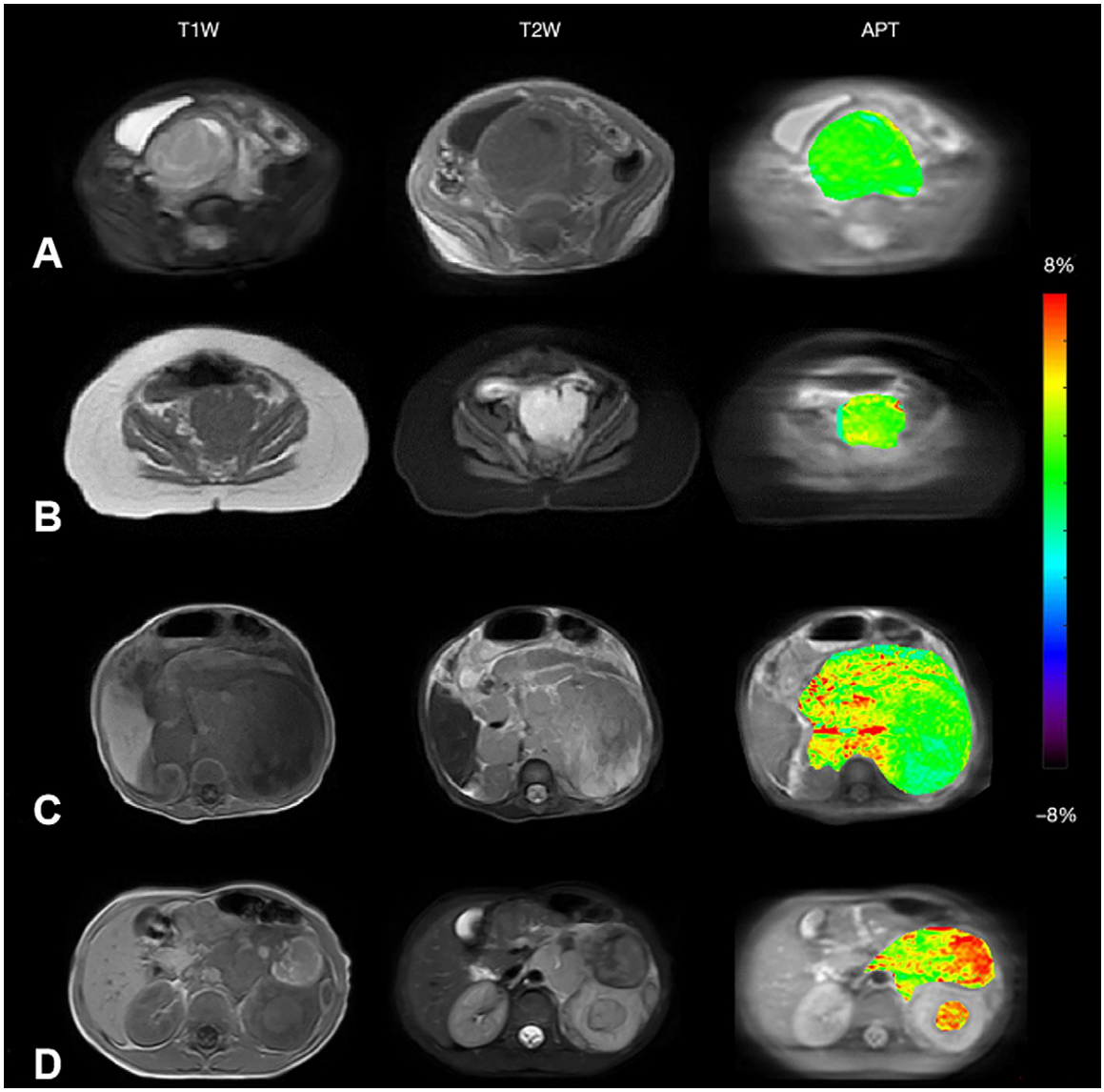

Figure 8: Axial T1-weighted (T1W), T2-weighted (T2W), and amide proton transfer (APT) images in patients with **(A)** very-low-risk, **(B)** low-risk, **(C)** intermediate-risk, and **(D)** high-risk neuroblastoma. (Adapted, under a CC BY-NC-ND 4.0 license, from reference 4.)

treatment, tissue T1 relaxation time may change. The treatment response can be monitored by performing native T1 mapping, allowing for adjustments to treatment plans. Zormpas-Petridis et al (53) found that native T1 mapping indicators correlated with the differentiation degree of tumor cells in a mouse model of neuroblastoma. Their study showed that regions with higher T1 values had an abundance of proliferating undifferentiated neuroblastoma cells, while regions with lower T1 values were richer in apoptotic or undifferentiated neuroblastoma cells. Additionally, native T1 mapping could detect the response of neuroblastoma to *MYCN*-targeted small molecule inhibitors. These results suggest that native T1 mapping not only helps assess the histologic characteristics of neuroblastoma but also assists in evaluating its response to targeted therapy.

Wang et al (54) discovered that the CT-based extracellular volume fraction of neuroblastoma was correlated with histologic characteristics, *MYCN* amplification, and risk stratification in neuroblastoma. Additionally, there was a correlation between CT-based extracellular volume fraction and the primary tumor response to treatment in neuroblastoma (55). Other studies have demonstrated that native T1 mapping indicators help quantitatively reflect the extracellular matrix (56). Thus, native T1 mapping may play a more important role in the diagnosis and risk stratification of neuroblastoma. However, further investigations are needed to confirm these hypotheses.

Conclusion

Although anatomic imaging aids in identifying IDRFs and evaluating treatment response in neuroblastoma, it has limitations in predicting prognosis. Specifically, the ability of IDRFs to predict overall survival in patients with neuroblastoma is moderate, highlighting the need for additional quantitative imaging biomarkers to enhance predictive tools. While quantitative MRI is promising, there is relatively less research and clinical validation in the context of neuroblastoma. More studies are needed to establish standardized protocols and validate its clinical utility in predicting prognosis in these patients. It is also worth noting that current studies on quantitative MRI in neuroblastoma do not include comparisons with anatomic imaging. Therefore, further investigation is needed to determine whether quantitative MRI can

provide independent imaging biomarkers with additional clinical value beyond anatomic imaging in neuroblastoma.

Disclosures of conflicts of interest: H.W. No relevant relationships. **J.C.** No relevant relationships.

References

1. Takita J. Molecular basis and clinical features of neuroblastoma. Japan Med Assoc J 2021;4(4):321–331.
2. Chen AM, Trout AT, Towbin AJ. A review of neuroblastoma image-defined risk factors on magnetic resonance imaging. Pediatr Radiol 2018;48(9):1337–1347.
3. Bagatell R, McHugh K, Naranjo A, et al. Assessment of primary site response in children with high-risk neuroblastoma: an international multicenter study. J Clin Oncol 2016;34(7):740–746.
4. Jia X, Wang W, Liang J, et al. Application of amide proton transfer imaging to pretreatment risk stratification of childhood neuroblastoma: comparison with neuron-specific enolase. Quant Imaging Med Surg 2023;13(5):3001–3012.
5. Peschmann AL, Beer M, Ammann B, et al. Quantitative DWI predicts event-free survival in children with neuroblastic tumours: preliminary findings from a retrospective cohort study. Eur Radiol Exp 2019;3(1):6.
6. Tas ML, Reedijk AMJ, Karim-Kos HE, et al. Neuroblastoma between 1990 and 2014 in the Netherlands: Increased incidence and improved survival of high-risk neuroblastoma. Eur J Cancer 2020;124:47–55.
7. Georgakis MK, Dessypris N, Baka M, et al. Neuroblastoma among children in Southern and Eastern European cancer registries: Variations in incidence and temporal trends compared to US. Int J Cancer 2018;142(10):1977–1985.
8. Campbell K, Siegel DA, Umaretiya PJ, et al. A comprehensive analysis of neuroblastoma incidence, survival, and racial and ethnic disparities from 2001 to 2019. Pediatr Blood Cancer 2024;71(1):e30732.
9. Liu S, Yin W, Lin Y, et al. Metastasis pattern and prognosis in children with neuroblastoma. World J Surg Oncol 2023;21(1):130.
10. Ritenour LE, Randall MP, Bosse KR, Diskin SJ. Genetic susceptibility to neuroblastoma: current knowledge and future directions. Cell Tissue Res 2018;372(2):287–307. [Published correction appears in Cell Tissue Res 2021;383(2):905.]
11. DuBois SG, Macy ME, Henderson TO. High-risk and relapsed neuroblastoma: toward more cures and better outcomes. Am Soc Clin Oncol Educ Book 2022;42(42):1–13.
12. Monclair T, Brodeur GM, Ambros PF, et al; INRG Task Force. The International Neuroblastoma Risk Group (INRG) staging system: an INRG Task Force report. J Clin Oncol 2009;27(2):298–303.
13. Cohn SL, Pearson AD, London WB, et al; INRG Task Force. The International Neuroblastoma Risk Group (INRG) classification system: an INRG Task Force report. J Clin Oncol 2009;27(2):289–297.
14. Jacobson JC, Clark RA, Chung DH. High-risk neuroblastoma: a surgical perspective. Children (Basel) 2023;10(2):388.
15. Kushner BH, Modak S, Kramer K, et al. Immunotherapy with anti-G_{D2} monoclonal antibody in infants with high-risk neuroblastoma. Int J Cancer 2023;152(2):259–266.
16. Saksiri P, Sripornsawan P, Kritsaneepaiboon S, Laochareonsuk W, Choochuen P, Sangkhathat S. Correlation between image-defined risk factors and surgical complications in patients with neuroblastoma: a retrospective study. Pediatr Surg Int 2023;39(1):70.
17. Wang H, Li T, Ni X, Chen X, He L, Cai J. Image-defined risk factors associated with MYCN oncogene amplification in neuroblastoma and their association with overall survival. Abdom Radiol (NY) 2024;49(6):1949–1960.
18. Chang S, Lin Y, Yang S, et al. Safety and feasibility of laparoscopic resection of abdominal neuroblastoma without image-defined risk factors: a single-center experience. World J Surg Oncol 2023;21(1):113.
19. Zenitani M, Yoshida M, Matsumoto S, et al. Feasibility and safety of laparoscopic tumor resection in children with abdominal neuroblastomas. Pediatr Surg Int 2023;39(1):91.
20. Parhar D, Joharifard S, Lo AC, Schlosser MP, Daodu OO. How well do image-defined risk factors (IDRFs) predict surgical outcomes and survival in patients with neuroblastoma? A systematic review and meta-analysis. Pediatr Surg Int 2020;36(8):897–907.
21. Wang H, Chen X, Zhu J, et al. Changes in image-defined risk factors with neoadjuvant chemotherapy in pediatric abdominal neuroblastoma. Abdom Radiol (NY) 2022;47(10):3520–3530.
22. Park JR, Bagatell R, Cohn SL, et al. Revisions to the International Neuroblastoma Response Criteria: A Consensus Statement From the National Cancer Institute Clinical Trials Planning Meeting. J Clin Oncol 2017;35(22):2580–2587.
23. Yeung F, Chung PH, Tam PK, Wong KK. Is complete resection of high-risk stage IV neuroblastoma associated with better survival? J Pediatr Surg 2015;50(12):2107–2111.
24. Mansfield SA, McCarville MB, Lucas JT Jr, et al. Impact of neoadjuvant chemotherapy on image-defined risk factors in high-risk neuroblastoma. Ann Surg Oncol 2022;29(1):661–670.
25. Mora J, Castañeda A, Colombo MC, et al. Clinical and pathological evidence of anti-GD2 immunotherapy induced differentiation in relapsed/refractory high-risk neuroblastoma. Cancers (Basel) 2021;13(6):1264.
26. Uhl M, Altehoefer C, Kontny U, Il'yasov K, Büchert M, Langer M. MRI-diffusion imaging of neuroblastomas: first results and correlation to histology. Eur Radiol 2002;12(9):2335–2338.
27. Gahr N, Darge K, Hahn G, Kreher BW, von Buiren M, Uhl M. Diffusion-weighted MRI for differentiation of neuroblastoma and ganglioneuroblastoma/ganglioneuroma. Eur J Radiol 2011;79(3):443–446.
28. Wen Y, Peng Y, Duan XM, Zhang N. Role of diffusion-weighted imaging in distinguishing thoracoabdominal neuroblastic tumours of various histological types and differentiation grades. J Med Imaging Radiat Oncol 2017;61(6):718–724.
29. Serin HI, Gorkem SB, Doganay S, et al. Diffusion weighted imaging in differentiating malignant and benign neuroblastic tumors. Jpn J Radiol 2016;34(9):620–624.
30. Neubauer H, Li M, Müller VR, Pabst T, Beer M. Diagnostic value of diffusion-weighted MRI for tumor characterization, differentiation and monitoring in pediatric patients with neuroblastic tumors. Rofo 2017;189(7):640–650.
31. Ghosh A, Yekeler E, Dalal D, Holroyd A, States L. Whole-tumour apparent diffusion coefficient (ADC) histogram analysis to identify MYCN-amplification in neuroblastomas: preliminary results. Eur Radiol 2022;32(12):8453–8462.
32. Aslan M, Aslan A, Arıöz Habibi H, et al. Diffusion-weighted MRI for differentiating Wilms tumor from neuroblastoma. Diagn Interv Radiol 2017;23(5):403–406.
33. Meeus EM, Zarinabad N, Manias KA, et al. Diffusion-weighted MRI and intravoxel incoherent motion model for diagnosis of pediatric solid abdominal tumors. J Magn Reson Imaging 2018;47(6):1475–1486.
34. Demir S, Altinkaya N, Kocer NE, Erbay A, Oguzkurt P. Variations in apparent diffusion coefficient values following chemotherapy in pediatric neuroblastoma. Diagn Interv Radiol 2015;21(2):184–188.
35. Privitera L, Hales PW, Musleh L, et al. Comparison between diffusion-weighted MRI and ^{123} I-mIBG uptake in primary high-risk neuroblastoma. J Magn Reson Imaging 2021;53(5):1486–1497.
36. Ishiguchi H, Ito S, Kato K, et al. Diagnostic performance of ^{18}F-FDG PET/CT and whole-body diffusion-weighted imaging with background body suppression (DWIBS) in detection of lymph node and bone metastases from pediatric neuroblastoma. Ann Nucl Med 2018;32(5):348–362.
37. Gassenmaier S, Bares R, Barreuther M, et al. ^{123}Iodine-metaiodobenzylguanidine scintigraphy versus whole-body magnetic resonance imaging with diffusion-weighted imaging in children with high-risk neuroblastoma - pilot study. Pediatr Radiol 2021;51(7):1223–1230.
38. Federau C. Measuring perfusion: intravoxel incoherent motion MR imaging. Magn Reson Imaging Clin N Am 2021;29(2):233–242.
39. Rosenkrantz AB, Padhani AR, Chenevert TL, et al. Body diffusion kurtosis imaging: Basic principles, applications, and considerations for clinical practice. J Magn Reson Imaging 2015;42(5):1190–1202.
40. Xiao Z, Tang Z, Qiang J, et al. Differentiation of olfactory neuroblastomas from nasal squamous cell carcinomas using MR diffusion kurtosis imaging and dynamic contrast-enhanced MRI. J Magn Reson Imaging 2018;47(2):354–361.
41. Winfield JM, Payne GS, deSouza NM. Functional MRI and CT biomarkers in oncology. Eur J Nucl Med Mol Imaging 2015;42(4):562–578.
42. Kohe SE, Bennett CD, Gill SK, Wilson M, McConville C, Peet AC. Metabolic profiling of the three neural derived embryonal pediatric tumors retinoblastoma, neuroblastoma and medulloblastoma, identifies distinct metabolic profiles. Oncotarget 2018;9(13):11336–11351.
43. Peet AC, McConville C, Wilson M, et al. 1H MRS identifies specific metabolite profiles associated with MYCN-amplified and non-amplified tumour subtypes of neuroblastoma cell lines. NMR Biomed 2007;20(7):692–700.
44. Lindskog M, Spenger C, Jarvet J, Gräslund A, Kogner P. Predicting resistance or response to chemotherapy by proton magnetic resonance spectroscopy in neuroblastoma. J Natl Cancer Inst 2004;96(19):1457–1466.
45. Morin CE, Hasweh R, Anton C, et al. Gadolinium-based contrast media does not improve the staging of neuroblastoma image-defined risk factors at diagnosis. Pediatr Blood Cancer 2024;71(1):e30724.
46. van Osch MJ, Teeuwisse WM, Chen Z, Suzuki Y, Helle M, Schmid S. Advances in arterial spin labelling MRI methods for measuring perfusion and collateral flow. J Cereb Blood Flow Metab 2018;38(9):1461–1480.
47. Harteveld AA, Littooij AS, van Noesel MM, van Stralen M, Bos C. Perfusion imaging of neuroblastoma and nephroblastoma in a paediatric population using pseudo-continuous arterial spin-labelling magnetic resonance imaging. MAGMA 2022;35(2):235–246. [Published correction appears in MAGMA 2022;35(2):247.]

48. Bellary A, Nowak C, Iwanicki I, et al. Non-viral nitric oxide-based gene therapy improves perfusion and liposomal doxorubicin sonopermeation in neuroblastoma models. Theranostics 2023;13(10):3402–3418.
49. Gao T, Zou C, Li Y, Jiang Z, Tang X, Song X. A brief history and future prospects of CEST MRI in clinical non-brain tumor imaging. Int J Mol Sci 2021;22(21):11559.
50. Kamimura K, Nakajo M, Yoneyama T, et al. Amide proton transfer imaging of tumors: theory, clinical applications, pitfalls, and future directions. Jpn J Radiol 2019;37(2):109–116.
51. Tanoue M, Saito S, Takahashi Y, et al. Amide proton transfer imaging of glioblastoma, neuroblastoma, and breast cancer cells on a 11.7 T magnetic resonance imaging system. Magn Reson Imaging 2019;62:181–190.
52. Jia X, Wang W, Liang J, et al. Risk stratification of abdominal tumors in children with amide proton transfer imaging. Eur Radiol 2022;32(4):2158–2167.
53. Zormpas-Petridis K, Poon E, Clarke M, et al. Noninvasive MRI native T_1 mapping detects response to *MYCN*-targeted therapies in the Th-*MYCN* model of neuroblastoma. Cancer Res 2020;80(16):3424–3435.
54. Wang H, Ding H, Xie M, et al. Correlations between contrast-enhanced CT-measured extracellular volume fraction, histopathological features, and MYCN amplification status in abdominal neuroblastoma: a retrospective study. Abdom Radiol (NY) 2023;48(11):3441–3448.
55. Wang H, Chen X, Xie M, Qin J, Li T, He L. Impact of pre-treatment extracellular volume fraction measured by computed tomography on response of primary lesion to preoperative chemotherapy in abdominal neuroblastoma. Clinics (São Paulo) 2024;79:100434.
56. Keller S, Borde T, Brangsch J, et al. Native T1 mapping magnetic resonance imaging as a quantitative biomarker for characterization of the extracellular matrix in a rabbit hepatic cancer model. Biomedicines 2020;8(10):412.